DESY 00-035 ISSN 0418-9833
March 2000

Measurement of Di-jet Cross-Sections in Photoproduction and Photon Structure

H1 Collaboration

Abstract

The production of hard di-jet events in photoproduction at HERA is dominated by resolved photon processes in which a parton in the photon with momentum fraction x_γ is scattered from a parton in the proton. These processes are sensitive to the quark and gluon content of the photon. The differential di-jet cross-section $\mathrm{d}\sigma/\mathrm{d}\log(x_\gamma)$ is presented here, measured in tagged photoproduction at HERA using data taken with the H1 detector, corresponding to an integrated luminosity of 7.2 pb^{-1}. Using a restricted data sample at high transverse jet energy, $E_{T,jet} > 6$ GeV, the effective parton density $f_{\gamma,eff}(x_\gamma) = [q(x_\gamma) + \bar{q}(x_\gamma) + 9/4\, g(x_\gamma)]$ in the photon in leading order QCD is measured down to x_γ= 0.05 from which the gluon density in the photon is derived.

Submitted to Physics Letters

C. Adloff[33], V. Andreev[24], B. Andrieu[27], V. Arkadov[35], A. Astvatsatourov[35], I. Ayyaz[28], A. Babaev[23], J. Bähr[35], P. Baranov[24], E. Barrelet[28], W. Bartel[10], U. Bassler[28], P. Bate[21], A. Beglarian[34], O. Behnke[10], C. Beier[14], A. Belousov[24], T. Benisch[10], Ch. Berger[1], G. Bernardi[28], T. Berndt[14], G. Bertrand-Coremans[4], J.C. Bizot[26], K. Borras[7], V. Boudry[27], W. Braunschweig[1], V. Brisson[26], H.-B. Bröker[2], D.P. Brown[21], W. Brückner[12], P. Bruel[27], D. Bruncko[16], J. Bürger[10], F.W. Büsser[11], A. Bunyatyan[12,34], S. Burke[17], H. Burkhardt[14], A. Burrage[18], G. Buschhorn[25], A.J. Campbell[10], J. Cao[26], T. Carli[25], S. Caron[1], E. Chabert[22], D. Clarke[5], B. Clerbaux[4], C. Collard[4], J.G. Contreras[7,41], J.A. Coughlan[5], M.-C. Cousinou[22], B.E. Cox[21], G. Cozzika[9], J. Cvach[29], J.B. Dainton[18], W.D. Dau[15], K. Daum[33,39], M. David[9,†], M. Davidsson[20], B. Delcourt[26], N. Delerue[22], R. Demirchyan[34], A. De Roeck[10,43], E.A. De Wolf[4], C. Diaconu[22], P. Dixon[19], V. Dodonov[12], K.T. Donovan[19], J.D. Dowell[3], A. Droutskoi[23], C. Duprel[2], J. Ebert[33], G. Eckerlin[10], D. Eckstein[35], V. Efremenko[23], S. Egli[37], R. Eichler[36], F. Eisele[13], E. Eisenhandler[19], M. Ellerbrock[13], E. Elsen[10], M. Erdmann[10,40,e], P.J.W. Faulkner[3], L. Favart[4], A. Fedotov[23], R. Felst[10], J. Feltesse[9], J. Ferencei[10], F. Ferrarotto[31], S. Ferron[27], M. Fleischer[10], G. Flügge[2], A. Fomenko[24], I. Foresti[37], J. Formánek[30], J.M. Foster[21], G. Franke[10], E. Gabathuler[18], K. Gabathuler[32], J. Garvey[3], J. Gassner[32], J. Gayler[10], R. Gerhards[10], S. Ghazaryan[34], A. Glazov[35], L. Goerlich[6], N. Gogitidze[24], M. Goldberg[28], C. Goodwin[3], I. Gorelov[23], C. Grab[36], H. Grässler[2], T. Greenshaw[18], R.K. Griffiths[19], G. Grindhammer[25], T. Hadig[1], D. Haidt[10], L. Hajduk[6], V. Haustein[33], W.J. Haynes[5], B. Heinemann[10], G. Heinzelmann[11], R.C.W. Henderson[17], S. Hengstmann[37], H. Henschel[35], R. Heremans[4], G. Herrera[7,41,k], I. Herynek[29], M. Hilgers[36], K.H. Hiller[35], C.D. Hilton[21], J. Hladký[29], P. Höting[2], D. Hoffmann[10], W. Hoprich[12], R. Horisberger[32], S. Hurling[10], M. Ibbotson[21], Ç. İşsever[7], M. Jacquet[26], M. Jaffre[26], L. Janauschek[25], D.M. Jansen[12], X. Janssen[4], V. Jemanov[11], L. Jönsson[20], D.P. Johnson[4], M.A.S. Jones[18], H. Jung[20], H.K. Kästli[36], D. Kant[19], M. Kapichine[8], M. Karlsson[20], O. Karschnick[11], O. Kaufmann[13], M. Kausch[10], F. Keil[14], N. Keller[13], J. Kennedy[18], I.R. Kenyon[3], S. Kermiche[22], C. Kiesling[25], M. Klein[35], C. Kleinwort[10], G. Knies[10], B. Koblitz[25], H. Kolanoski[38], S.D. Kolya[21], V. Korbel[10], P. Kostka[35], S.K. Kotelnikov[24], M.W. Krasny[28], H. Krehbiel[10], J. Kroseberg[37], D. Krücker[38], K. Krüger[10], A. Küpper[33], T. Kuhr[11], T. Kurča[35], R. Kutuev[12], W. Lachnit[10], R. Lahmann[10], D. Lamb[3], M.P.J. Landon[19], W. Lange[35], T. Lastovicka[30], A. Lebedev[24], B. Leißner[1], V. Lemaitre[10], R. Lemrani[10], V. Lendermann[7], S. Levonian[10], M. Lindstroem[20], G. Lobo[26], E. Lobodzinska[10], B. Lobodzinski[6,10], N. Loktionova[24], V. Lubimov[23], S. Lüders[36], D. Lüke[7,10], L. Lytkin[12], N. Magnussen[33], H. Mahlke-Krüger[10], N. Malden[21], E. Malinovski[24], I. Malinovski[24], R. Maraček[25], P. Marage[4], J. Marks[13], R. Marshall[21], H.-U. Martyn[1], J. Martyniak[6], S.J. Maxfield[18], T.R. McMahon[18], A. Mehta[5], K. Meier[14], P. Merkel[10], F. Metlica[12], A. Meyer[10], H. Meyer[33], J. Meyer[10], P.-O. Meyer[2], S. Mikocki[6], D. Milstead[18], T. Mkrtchyan[34], R. Mohr[25], S. Mohrdieck[11], M.N. Mondragon[7], F. Moreau[27], A. Morozov[8], J.V. Morris[5], D. Müller[37], K. Müller[13], P. Murín[16,42], V. Nagovizin[23], B. Naroska[11], J. Naumann[7], Th. Naumann[35], I. Négri[22], P.R. Newman[3], H.K. Nguyen[28], T.C. Nicholls[3], F. Niebergall[11], C. Niebuhr[10], O. Nix[14], G. Nowak[6], T. Nunnemann[12], J.E. Olsson[10], D. Ozerov[23], V. Panassik[8], C. Pascaud[26], S. Passaggio[36], G.D. Patel[18], E. Perez[9], J.P. Phillips[18], D. Pitzl[10], R. Pöschl[7], I. Potachnikova[12], B. Povh[12], K. Rabbertz[1], G. Rädel[9], J. Rauschenberger[11], P. Reimer[29], B. Reisert[25], D. Reyna[10], S. Riess[11], E. Rizvi[3], P. Robmann[37], R. Roosen[4], A. Rostovtsev[23,10], C. Royon[9], S. Rusakov[24], K. Rybicki[6], D.P.C. Sankey[5], J. Scheins[1], F.-P. Schilling[13], S. Schleif[14], P. Schleper[13], D. Schmidt[33],

D. Schmidt[10], L. Schoeffel[9], A. Schöning[36], T. Schörner[25], V. Schröder[10], H.-C. Schultz-Coulon[10], K. Sedlak[29], F. Sefkow[37], V. Shekelyan[25], I. Sheviakov[24], L.N. Shtarkov[24], G. Siegmon[15], P. Sievers[13], Y. Sirois[27], T. Sloan[17], P. Smirnov[24], M. Smith[18], V. Solochenko[23], Y. Soloviev[24], V. Spaskov[8], A. Specka[27], H. Spitzer[11], R. Stamen[7], J. Steinhart[11], B. Stella[31], A. Stellberger[14], J. Stiewe[14], U. Straumann[37], W. Struczinski[2], J.P. Sutton[3], M. Swart[14], M. Taševský[29], V. Tchernyshov[23], S. Tchetchelnitski[23], G. Thompson[19], P.D. Thompson[3], N. Tobien[10], D. Traynor[19], P. Truöl[37], G. Tsipolitis[36], J. Turnau[6], J.E. Turney[19], E. Tzamariudaki[25], S. Udluft[25], A. Usik[24], S. Valkár[30], A. Valkárová[30], C. Vallée[22], P. Van Mechelen[4], Y. Vazdik[24], G. Villet[9], S. von Dombrowski[37], K. Wacker[7], R. Wallny[13], T. Walter[37], B. Waugh[21], G. Weber[11], M. Weber[14], D. Wegener[7], A. Wegner[11], T. Wengler[13], M. Werner[13], L.R. West[3], G. White[17], S. Wiesand[33], T. Wilksen[10], M. Winde[35], G.-G. Winter[10], C. Wissing[7], M. Wobisch[2], H. Wollatz[10], E. Wünsch[10], J. Žáček[30], J. Zálešák[30], Z. Zhang[26], A. Zhokin[23], P. Zini[28], F. Zomer[26], J. Zsembery[9] and M. zur Nedden[10]

[1] *I. Physikalisches Institut der RWTH, Aachen, Germany*[a]
[2] *III. Physikalisches Institut der RWTH, Aachen, Germany*[a]
[3] *School of Physics and Space Research, University of Birmingham, Birmingham, UK*[b]
[4] *Inter-University Institute for High Energies ULB-VUB, Brussels; Universitaire Instelling Antwerpen, Wilrijk; Belgium*[c]
[5] *Rutherford Appleton Laboratory, Chilton, Didcot, UK*[b]
[6] *Institute for Nuclear Physics, Cracow, Poland*[d]
[7] *Institut für Physik, Universität Dortmund, Dortmund, Germany*[a]
[8] *Joint Institute for Nuclear Research, Dubna, Russia*
[9] *DSM/DAPNIA, CEA/Saclay, Gif-sur-Yvette, France*
[10] *DESY, Hamburg, Germany*[a]
[11] *II. Institut für Experimentalphysik, Universität Hamburg, Hamburg, Germany*[a]
[12] *Max-Planck-Institut für Kernphysik, Heidelberg, Germany*[a]
[13] *Physikalisches Institut, Universität Heidelberg, Heidelberg, Germany*[a]
[14] *Kirchhoff-Institut für Physik, Universität Heidelberg, Heidelberg, Germany*[a]
[15] *Institut für experimentelle und angewandte Physik, Universität Kiel, Kiel, Germany*[a]
[16] *Institute of Experimental Physics, Slovak Academy of Sciences, Košice, Slovak Republic*[e,f]
[17] *School of Physics and Chemistry, University of Lancaster, Lancaster, UK*[b]
[18] *Department of Physics, University of Liverpool, Liverpool, UK*[b]
[19] *Queen Mary and Westfield College, London, UK*[b]
[20] *Physics Department, University of Lund, Lund, Sweden*[g]
[21] *Department of Physics and Astronomy, University of Manchester, Manchester, UK*[b]
[22] *CPPM, CNRS/IN2P3 - Univ Mediterranee, Marseille - France*
[23] *Institute for Theoretical and Experimental Physics, Moscow, Russia*
[24] *Lebedev Physical Institute, Moscow, Russia*[e,h]
[25] *Max-Planck-Institut für Physik, München, Germany*[a]
[26] *LAL, Université de Paris-Sud, IN2P3-CNRS, Orsay, France*
[27] *LPNHE, École Polytechnique, IN2P3-CNRS, Palaiseau, France*
[28] *LPNHE, Universités Paris VI and VII, IN2P3-CNRS, Paris, France*
[29] *Institute of Physics, Academy of Sciences of the Czech Republic, Praha, Czech Republic*[e,i]
[30] *Faculty of Mathematics and Physics, Charles University, Praha, Czech Republic*[e,i]

[31] *INFN Roma 1 and Dipartimento di Fisica, Università Roma 3, Roma, Italy*
[32] *Paul Scherrer Institut, Villigen, Switzerland*
[33] *Fachbereich Physik, Bergische Universität Gesamthochschule Wuppertal, Wuppertal, Germany*[a]
[34] *Yerevan Physics Institute, Yerevan, Armenia*
[35] *DESY, Zeuthen, Germany*[a]
[36] *Institut für Teilchenphysik, ETH, Zürich, Switzerland*[j]
[37] *Physik-Institut der Universität Zürich, Zürich, Switzerland*[j]

[38] *Present address: Institut für Physik, Humboldt-Universität, Berlin, Germany*
[39] *Also at Rechenzentrum, Bergische Universität Gesamthochschule Wuppertal, Wuppertal, Germany*
[40] *Also at Institut für Experimentelle Kernphysik, Universität Karlsruhe, Karlsruhe, Germany*
[41] *Also at Dept. Fis. Ap. CINVESTAV, Mérida, Yucatán, México*[k]
[42] *Also at University of P.J. Šafárik, Košice, Slovak Republic*
[43] *Also at CERN, Geneva, Switzerland*

† *Deceased*

[a] *Supported by the Bundesministerium für Bildung, Wissenschaft, Forschung und Technologie, FRG, under contract numbers 7AC17P, 7AC47P, 7DO55P, 7HH17I, 7HH27P, 7HD17P, 7HD27P, 7KI17I, 6MP17I and 7WT87P*
[b] *Supported by the UK Particle Physics and Astronomy Research Council, and formerly by the UK Science and Engineering Research Council*
[c] *Supported by FNRS-FWO, IISN-IIKW*
[d] *Partially Supported by the Polish State Committee for Scientific Research, grant No. 2P0310318 and SPUB/DESY/P-03/DZ 1/99*
[e] *Supported by the Deutsche Forschungsgemeinschaft*
[f] *Supported by VEGA SR grant no. 2/5167/98*
[g] *Supported by the Swedish Natural Science Research Council*
[h] *Supported by Russian Foundation for Basic Research grant no. 96-02-00019*
[i] *Supported by GA AVČR grant number no. A1010821*
[j] *Supported by the Swiss National Science Foundation*
[k] *Supported by CONACyT*

1 Introduction

The interaction of electrons and protons at the HERA collider is dominated by photoproduction processes in which quasireal photons emitted by the electrons interact with the protons. The center of mass energies in the γp system extend to 300 GeV. A fraction of these events has large transverse energy in the final state and contains jets. Previous studies of hard γp scattering processes by H1 [1–3] and ZEUS [4] have shown that the photoproduction of jets can be described in perturbative QCD. The photon interacts either directly with a parton from the proton, or it develops hadronic structure and one of its own partons interacts with one of those from the proton. The former are referred to as direct interactions, whereas the latter are referred to as resolved interactions.

Jet cross-section predictions are obtained to leading order (LO) in the strong coupling constant as a convolution of the hard scattering cross-sections calculated at the tree level with the parton densities in the photon and the proton. The partons leaving the hard scattering reaction are identified with jets. In the kinematic range of the present analysis the parton densities in the proton are rather well known and the quark densities of the photon have been determined from two-photon processes at e^+e^- colliders. The measurement of the di-jet cross-section can therefore be used to determine the gluon distribution in the photon.

From previous studies [2, 5] it is known that the energy flow in the events of interest here is complicated by a large "underlying event" energy, which can be described as arising from multiple interactions. That is, in addition to the primary hard interaction, further interactions occur between partons in the proton and photon remnants. Modelling of higher order QCD effects using parton showers is also important if an accurate description of the energy flow in and around the jets is to be obtained. Current Monte Carlo (MC) models including such effects are based on LO QCD matrix element calculations; NLO predictions are available at the parton level only.

The analysis described in this paper is similar to that presented in an earlier publication [2]. However, the data used now correspond to an integrated luminosity of 7.2 pb^{-1} as opposed to 0.29 pb^{-1}. Its main emphasis is on the study of di-jet production at small x_γ where gluons in the photon are expected to make the largest contribution to the cross-section. The data in this kinematic region are strongly affected by non-perturbative effects as discussed in detail below. We therefore limit ourselves here to a LO QCD analysis of the parton distributions in the photon. A NLO analysis of di-jet events in photoproduction has been published recently by the ZEUS collaboration [6] for a high cut in transverse jet energy $E_T > 11$ GeV. In this kinematic region of large x_γ, where the influence of the underlying event energy is reduced, the quark rather than the gluon content of the photon is expected to dominate the cross-section.

2 The H1 Detector

A detailed description of the H1 detector can be found elsewhere [7]. Here we describe only those components which are important for this analysis.

The H1 central tracking system is mounted coaxially around the beam-line and covers polar angles θ, measured with respect to the proton beam direction, in the range $20^\circ < \theta < 160^\circ$. Momentum measurements of charged particles are provided by two cylindrical drift chambers. The central tracking system is complemented at two radii by z- drift chambers, which provide accurate measurements of the z coordinate along the beam line of charged particle tracks, and multiwire proportional chambers (MWPCs), which allow triggering on central tracks. In the present analysis the tracking detectors are used to define the vertex position along the beam axis and to improve the measurement of the hadronic energy flow at low hadron energies.

The tracking system is surrounded by a highly segmented liquid argon (LAr) sampling calorimeter with an inner electromagnetic section consisting of lead absorber plates with a total depth of 20 to 30 radiation lengths and an outer hadronic section with steel absorber plates. The LAr calorimeter covers polar angles between 4° and 154° with full azimuthal acceptance. The total depth of the calorimeter varies between 4.5 and 8 hadronic interaction lengths. The energy resolution was measured to be $\sigma(E)/E \approx 0.12/\sqrt{E}$ for electrons and $\sigma(E)/E \sim 0.5/\sqrt{E}$ for hadrons (E in GeV) in test beam experiments. The absolute energy scale is known for the present data sample to a precision of 1 to 3% for positrons and 4% for hadrons. The region $153^\circ < \theta < 177.8^\circ$ is covered by a lead/scintillating-fibre calorimeter.

The luminosity determination is based on the measurement of the bremsstrahlung process, $ep \to ep\gamma$, using the small angle photon detector ($z = -103$ m), and by detecting the scattered positron in the small angle electron detector ($z = -33$ m) where z is the coordinate along the beam line with the nominal vertex at the origin. Both detectors are crystal Čerenkov calorimeters with an energy resolution of $\sigma(E)/E \approx 0.22/\sqrt{E}$. The luminosity is determined to an accuracy of 2% for the data sample used in this analysis. The small angle electron detector is used in the present analysis also to tag photoproduction events.

3 Event Selection and Kinematic Reconstruction

The events used in this analysis were taken during the 1996 running period, in which HERA collided 820 GeV protons with 27.5 GeV positrons.

The transverse jet energies required in this analysis are as low as 4 GeV. In order to improve the jet energy resolution at low jet energies the energy flow is reconstructed by combining the energy measurements made in the LAr calorimeter with the measured momenta of spatially associated charged tracks with transverse momenta smaller than 1.5 GeV, avoiding double counting. More details are given in [8].

Events were selected according to the following requirements:

1. The event is triggered by a combination of trigger signals from the small angle electron detector and from charged tracks in the central detectors with a minimum requirement on their transverse momentum of about 300 MeV.

2. The scattered positron is detected and measured in the small angle electron detector in order to ensure a low photon virtuality ($Q^2 < 0.01$ GeV^2). The energy fraction y_e

carried by the radiated photon is restricted to the range $0.5 < y_e < 0.7$, where y_e is reconstructed from the energy of the scattered positron. The lower cut on y_e ensures that a high momentum photon enters the hard scattering process such that the detector acceptance for the two hard jets is large; the upper cut is required by the acceptance of the small angle electron detector.

3. At least two jets with transverse energy $E_{T,jet} > 4$ GeV and an invariant jet-jet mass $M_{1,2} > 12$ GeV have to be found using a cone algorithm [9] in the region $-0.5 < \eta_{jet} < 2.5$. Here η_{jet} is the pseudorapidity in the laboratory and positive η corresponds to the direction of the outgoing proton. A small cone radius of $R = 0.7$ in the $\eta - \phi$ plane is used to reduce the effects of the underlying event energy on the jet energy measurement. The two jets with highest transverse energy are associated to the hard scattering process.

4. The difference in pseudorapidity between the jets is restricted to $|\eta_{jet1} - \eta_{jet2}| < 1$. This cut reduces the background of events where one jet is in the beam pipe and a second jet, not associated with the hard scattering process, is found instead.

Using these cuts 1889 di-jet events remain. The longitudinal momentum fraction of the incident parton in the photon is estimated using y_e and the transverse energies and pseudorapidities of the two jets with the highest E_T,

$$x_{\gamma,jets} = \frac{E_{T,jet1}e^{-\eta_{jet1}} + E_{T,jet2}e^{-\eta_{jet2}}}{2\, y_e\, E_{e,0}}, \tag{1}$$

where $E_{e,0}$ denotes the electron beam energy. In the selected event sample, x_γ is limited to the range $x_{\gamma,jets} > 0.03$ as a result of the cuts on the transverse energy, on the invariant mass of the jets, on the pseudorapidity and on y_e.

The trigger efficiency is monitored in the data by using an independent calorimetric reference trigger. The efficiency ranges from 90% at high $x_{\gamma,jets}$ to 65% at low $x_{\gamma,jets}$, and is well described by the detector simulation. An error of $\pm 5\%$ is assigned to the trigger efficiency.

4 Monte Carlo Generators for Hard γp Processes

The analysis uses simulated events to correct the measurements for detector effects, and to further compare the data with perturbative QCD predictions for the hard parton scattering and different models for multiple interactions. The Monte Carlo generators used in this analysis are PHOJET [10] and PYTHIA [11]. Both use LO QCD matrix elements for the hard scattering subprocesses. Initial and final state parton radiation and the string fragmentation model are included as implemented in the JETSET program [12]. The two Monte Carlo generators differ in the treatment of multiple interactions and the transition from hard to soft processes at low transverse parton momentum $\hat{p}_T$. The hard parton-parton cross-section diverges towards low $\hat{p}_t$ and therefore needs a regularisation to normalise to the measured total cross-section. This regularisation is achieved for PHOJET by a simple cut-off at $\hat{p}_t = 2.5$ GeV. For the PYTHIA generator we have chosen the option to use a damping factor $\hat{p}_t^2/(\hat{p}_t^2 + \hat{p}_{0t}^2)$ where $\hat{p}_{0t}$ was taken to be 1.55 GeV. [1]

The PHOJET event generator simulates in a consistent way all components that contribute to the total photoproduction cross-section. PHOJET incorporates detailed simulations of both multiple soft and hard parton interactions on the basis of a unitarisation scheme.

The PYTHIA 5.7 event generator uses LO QCD calculations to simulate both the primary parton-parton scattering process and multiple parton interactions. The latter are considered to result from the scattering of partons from the photon and proton remnants. The final state partons are required to have a transverse momentum of at least 1.2 GeV in all cases.

For both Monte Carlo models the factorisation and renormalisation scales were set to the transverse momentum $\hat{p}_t$ of the scattered partons. GRV92-LO [13] parton distribution functions for the proton and photon were used for the generation of the events.

5 Energy Flow and Jet Correlations

A precise measurement of the transverse jet energy $E_{T,jet}$ is very important because the measured transverse jet energy distribution falls roughly as $(E_{T,jet})^{-5.5}$. Therefore a poor description of the energy flow around the jet leads to severe systematic biases in the determination of cross-sections.

The transverse energy flow is well described by both Monte Carlo simulations within the jet cone. They differ, however, outside the jets: PYTHIA slightly overestimates and PHOJET underestimates the transverse energy [14]. Remaining differences between the two Monte Carlo models are used to estimate the systematic error of the jet reconstruction due to the underlying event energy. The transverse energy outside the jet cones depends mainly on η because the energy available for multiple interactions is large for small x_γ, i.e. large η, where the photon spectator has large fractional momentum $1 - x_\gamma$. The average transverse energy density (per unit area in $\eta - \phi$) outside the jets in the interval $-1 < \eta - \eta_{jet} < 1$ is shown in Figure 1 versus η_{jet} compared to the predictions of the two Monte Carlo models. This "pedestal" energy $E_{T,Ped}$ is calculated as follows. For every jet the transverse energy is summed in the region Ω with area A defined by $-1 < \eta - \eta_{jet} < 1$ and $-\pi < \phi - \phi_{jet} < \pi$ around the analysed jet but excluding the jets themselves using a cone radius R=1.0. $E_{T,Ped}$ is finally given by:

$$E_{T,Ped} = \frac{1}{A} \sum_{\Omega} E_T \tag{2}$$

The average transverse energy density measured outside of the jets (pedestal energy) is as high as 1.4 GeV at large η_{jet} and can therefore give, at small jet energies, a substantial contribution to the transverse energy of a jet. A detailed study of the jet-jet correlations using the two Monte Carlo models shows good agreement between data and MC which justifies the use of these LO QCD Monte Carlo generators for the analysis.

[1] This regularisation corresponds to a model with variable impact parameter for multiple parton interactions as explained in reference [11], section 11.2.

6 Di-jet Cross-Section for $E_{T,jet} > 4$ GeV

Jets at the detector level are reconstructed using calorimeter clusters and tracks. Monte Carlo events offer both the possibility to reconstruct jets at the detector level and to reconstruct jets using the generated hadrons. The reconstructed jets are then used to calculate x_γ at the detector level (termed $x_{\gamma,det}$) and at the hadron jet level (termed $x_{\gamma,jets}$). The correlation between these two quantities is used to unfold [15] the measured $x_{\gamma,det}$ distribution to the hadron jet level in bins of $x_{\gamma,jets}$. This correlation can be characterised by a Gaussian distribution in the quantity $(\log(x_{\gamma,det}) - \log(x_{\gamma,jets}))$ with a dispersion of $\sigma \approx 0.12$ and small non-Gaussian tails. Finally, the differential cross-section $\mathrm{d}\sigma/\mathrm{d}\log(x_{\gamma,jets})$ is calculated. After reweighting the distributions according to the new cross-section derived during unfolding, both Monte Carlo simulations describe all aspects of the measured data distributions in the detector equally well.

The dominant systematic error (up to 24% at low x_γ) results from the uncertainty on the hadronic energy scale of $\pm 4\%$. The stability of the unfolding procedure is studied by starting with very different cross-sections in the Monte Carlo simulation. This results in changes of the unfolded cross-section of less than 10%. The jet cross section has been determined using both Monte Carlo simulations (PYTHIA and PHOJET) and by using renormalisation and factorisation scales $0.5\ \hat{p}_t$ in addition to the default choices $\hat{p}_t$ for the unfolding. The differences of these cross-sections are used to evaluate the systematic errors of the corrections for detector acceptance and resolution. The detector corrections are found to differ by up to 10%. Additional experimental uncertainties arise from the trigger efficiency (5%) and the acceptance of the small angle electron detector and from the luminosity measurement (combined error 6%). All systematic errors are added in quadrature.

The di-jet cross-section $\mathrm{d}\sigma/\mathrm{d}\log(x_{\gamma,jets})$ is shown in Figure 2 and Table 1 where the data points are averages of the results obtained using the two Monte Carlo simulations for unfolding. The measurement is made in the kinematic region $E_{T,jet} > 4$ GeV, $M_{1,2} > 12$ GeV, $-0.5 < \eta_{jet} < 2.5$, $|\eta_{jet1} - \eta_{jet2}| < 1$ and $0.5 < y_e < 0.7$, where the kinematic variables are calculated using hadron level jets. The inner error bars reflect the statistical errors and the outer error bars show the statistical and systematic errors added in quadrature. This cross-section determination relies on an adequate description of the energy flow and of the angular correlations of the jets, both of which are achieved by the PYTHIA and PHOJET Monte Carlo simulations as discussed in section 5. Remaining differences outside the jet cones between data and either of the Monte Carlo simulations are comparable to the difference between the two Monte Carlo simulations. The systematic error associated with the uncertainty in the description of the energy flow, especially of the underlying event energy, is therefore estimated as half the difference of the results obtained when unfolding with the alternative Monte Carlo simulations. It amounts to 10 to 15 %.

The absolute predictions of the PHOJET and PYTHIA models using the same parton density functions for the photon and the proton and the same factorisation and renormalisation scales are shown in Figure 2 in comparison to the data. The two predictions should be the same if this low E_T jet sample were dominated by the effects of hard scattering. However, they differ by almost a factor 2 for $x_\gamma < 0.5$. This can be traced back to the parton transverse momentum spectra of the selected di-jet events which differ greatly for PYTHIA and PHOJET at low $\hat{p}_t$ due to the different regularisation procedures. PYTHIA predicts a much larger fraction of di-jet events than PHOJET with parton $\hat{p}_t$ between 2 and 4 GeV. Such partons produce jets with

$E_{T,jet} > 4$ GeV because of a large underlying event energy in the jet cone. We conclude that this event sample is strongly influenced by effects such as the regularisation procedure and the underlying event energy which makes a comparison to perturbative QCD predictions difficult. However, both models lead to a comparable good description of all aspects of the data once the predictions are reweighted to the measured x_γ distribution. Therefore the measured cross-section is a solid experimental result which can be compared to every model which gives a complete description of hard γp processes.

7 Analysis of Di-jet events for $E_{T,jet} > 6$ GeV

The determination of cross-sections usable for perturbative QCD analysis requires a data sample which is dominated by the effects of the partons from the hard scattering process. A more restrictive data selection is therefore used for the subsequent analysis steps.

The initial selection used here is as described in the previous section, but without the application of the jet-jet mass cut, which becomes ineffective for the increased E_T cut (see below). The following further requirements are then made:

1. The transverse energy in the jet cone for each jet is corrected for the average expected underlying event energy $E_{T,Ped}$ as function of η_{jet} (Figure 1). To do this, the average transverse energy density, as determined outside the jet cone using the Monte Carlo simulations, is subtracted from the measured energy in the cone. Monte Carlo studies show that this simple procedure leads to good agreement between the average jet and parton energies and at the same time improves the energy correlation significantly for individual events.

   After this subtraction the remaining transverse jet energy has to be larger than 6 GeV. This procedure reduces non-perturbative effects much more effectively than just raising the cut on $E_{T,jet}$.

2. The pseudorapidity of each jet has to satisfy the requirement $\eta_{jet} > -0.9 - \ln[x_{\gamma,jets}]$. While this cut hardly affects genuine di-jet events with $E_{T,jet} > 6$ GeV and $|\eta_{jet1} - \eta_{jet2}| < 1$, it eliminates a large fraction of those events where one of the two jets used to reconstruct x_γ is not associated with the hard scattering process.

These additional cuts are introduced to achieve a good correlation between the measured and true values of x_γ. They also reduce the differences in the parton distributions of the two Monte Carlo event samples. The selected di-jet sample contains 750 events.

7.1 Di-jet Cross-Section for $E_{T,jet} > 6$ GeV

The cross-section $\mathrm{d}\sigma/\mathrm{d}\log(x_{\gamma,jets})$ is determined from the event sample with the jet transverse energy cut $E_{T,jet} > 6$ GeV at the hadron level after pedestal energy subtraction. The result is shown in Figure 3 and Table 1 where the data points are obtained by averaging the results from the two Monte Carlo used for unfolding. In Figure 3 the data are compared to the predictions of the two Monte Carlo simulations using the GRV92 LO structure functions and $\hat{p_t}$ for the renormalisation and factorisation scales. For PHOJET the contributions of resolved photon interactions due to quarks and gluons from the photon and from direct photon interactions are shown separately. The higher E_T cut, combined with the pedestal subtraction, strongly depopulates the low x_γ region and therefore also the region where gluons from the photon dominate. Nevertheless, the data remain sensitive to the gluon distribution down to x_γ= 0.05. The differences between the PYTHIA and PHOJET predictions based on the same parton densities and using the same scales are now at a level between 10 and 40%.

7.2 The Effective Parton Distribution

The di-jet cross-section in LO QCD is given by a sum of direct and resolved photon contributions. The direct photon contribution depends only on the well known parton distributions in the proton and can therefore be predicted. The resolved part of the di-jet cross-section in LO QCD is a sum of quark-quark (qq), gluon-quark (gq) and gluon-gluon (gg) scattering processes with different angular distributions and weights. To a good approximation, however, the differential cross-section, in the $\Delta\eta$ range chosen for this analysis, can be described with a single effective subprocess using effective parton distributions for the photon and proton and a single differential parton-parton angular distribution $\mathrm{d}\hat{\sigma}/\mathrm{d}\cos\hat{\Theta}$ [16]. This is because the angular distribution is very similar for the largest contributing subprocesses within the present $\Delta\eta$ range (gg, gq and $qq \to qq$). For resolved processes the differential cross-section can therefore be approximately expressed as

$$\frac{\mathrm{d}^4\sigma^{ep}}{\mathrm{d}y\,\mathrm{d}x_\gamma\,\mathrm{d}x_p\,\mathrm{d}\cos\hat{\Theta}} = \frac{1}{32\pi s_{ep}}\frac{f_{\gamma/e}}{y}\frac{f_{\gamma,eff}(x_\gamma)f_{p,eff}(x_p)}{x_\gamma x_p}\frac{\mathrm{d}\hat{\sigma}}{\mathrm{d}\cos\hat{\Theta}}$$

Here the effective parton distributions for the photon and proton can be written

$$f_{\gamma,eff}(x_\gamma) = [q(x_\gamma) + \bar{q}(x_\gamma) + 9/4\ g(x_\gamma)]$$

$$f_{p,eff}(x_p) = [q(x_p) + \bar{q}(x_p) + 9/4\ g(x_p)]$$

$f_{\gamma/e}$ is the photon flux and s_{ep} is the center of mass energy squared of the ep system. The quark densities $q(x)$ comprise the sum over all flavours. Since the parton densities in the proton are well constrained, the effective parton density in the photon can be determined from the measured cross-section. Monte Carlo studies [14] show that the correlation between $x_{\gamma,jets}$ as reconstructed with hadron jets and the generated momentum fraction x_γ of the parton entering the hard scattering process from the photon side for both PYTHIA and PHOJET is rather good. It can be characterised by a Gaussian distribution of the quantity $(\log(x_{\gamma,jets}) - \log(x_\gamma))$ with a dispersion of $\sigma \approx 0.2$ and only small non-Gaussian tails over the full measured range of x_γ. This correlation is used to correct the measured jet cross-section for the effects of hadronisation and underlying event energy (which is only subtracted on average) using the unfolding method of [15]. During the unfolding procedure the direct and resolved photon contributions are calculated keeping all parton densities in the proton fixed to the GRV92 LO parton distributions [13], while the effective parton density in the photon is adjusted to get best agreement with the measured x_γ distribution. This determines the effective parton density in the photon.

After unfolding and reweighting to the new effective parton density, all Monte Carlo distributions are in good agreement with the data for both models [14]. This demonstrates that it is possible in a leading order Monte Carlo model for the hard scattering process to get a good description of the observed di-jet events when the optimised photon parton densities derived from our data are used.

Figure 4 and Table 2 show the measured effective parton density of the photon multiplied by $\alpha^{-1}x_\gamma$, where α is the fine structure constant. The LO QCD expectation for the direct photon contribution, as given by the Monte Carlo simulations, has been subtracted. The magnitude and distribution of this contribution can be seen in Figure 3. It amounts to about 23% of the selected di-jet events. The measured points correspond to an average scale $\hat{p_t}^2 = 74$ GeV^2 as determined from the $\hat{p_t}$ of the partons in the weighted Monte Carlo sample which describes the data distributions. Both statistical and total errors are given. Systematic errors have been determined using the method outlined in section 6. A systematic error due to model uncertainties in the x_γ correlation is added. This error is dominated by the subtraction of the underlying event energy and taken to be half the difference between the effective parton distributions using PYTHIA or PHOJET respectively for the unfolding. It amounts to 15 to 20%. The data points of Figure 4 and Table 2 are finally obtained by averaging the results obtained using the two Monte Carlo simulations for unfolding.

The measured effective parton distribution is compared to the GRV92 LO parametrisation of the parton densities in the photon which is obtained by a fit to e^+e^- two-photon data alone [13]. These data constrain the quark density in the photon, but give only indirect information on the gluon distribution via the observed scaling violations. The contribution of quarks plus antiquarks in the photon as given by the GRV92 parametrisation is shown separately. It includes the charm contribution (about 25% of the quark contribution) as calculated for γp interactions. The predicted quark plus antiquark contribution describes the data well at the highest values of x_γ but falls far below at small x_γ. Within LO QCD the difference can only be attributed to a gluon contribution which thus is shown to rise strongly towards low x_γ.

The extracted effective parton density constitutes the main result of this analysis at the parton level since, in contrast to the gluon density, it can be extracted from our data alone.

7.3 The Gluon Distribution

Since the quark density in the photon is well constrained by studies of photon-photon collisions in e^+e^- data [17] it can be subtracted from the measured effective parton density within the present LO QCD approach. The subtraction is performed using the GRV92 LO parton distributions which are in good agreement with the data and with other parametrisations. The resulting gluon distribution in the photon is shown in Figure 5 and Table 2. The total error includes the uncertainty of the quark plus antiquark contribution in the photon which is known with an error of less than 30% for $0.1 < x_\gamma < 0.8$ as derived directly from the measurement [18]. This uncertainty increases up to 60% at the smallest $x_\gamma$values considered here. This conservative error estimate covers also the uncertainty in the calculated charm contribution.

The gluon distribution is only large for small x_γ as expected. The present measurement is in good agreement with an earlier H1 measurement [19] based on high transverse momentum tracks in photoproduction at scales ${\hat{p}_t}^2 = 38$ GeV^2 where systematic uncertainties are very different. The analysis based on high transverse momentum tracks has the advantage that it is hardly affected by the underlying event energy. However, in such an analysis it is not possible to define a quantity which is strongly correlated to x_γ. This made the unfolding procedure less effective and required coarse binning in x_γ.

The measurements are compared to LO parametrisations of the gluon distribution. Of the two older parametrisations, that of GRV92 LO [13] gives best agreement with the data and has been used throughout this paper for comparisons of the data with Monte Carlo predictions, whereas the parametrisation of LAC1 [20] shows a too steep rise at small x_γ. The more recent parametrisations GRS99 [21] and SaS1D [22] agree very well with each other but fall below the measured distribution.

8 Conclusions

Two new measurements of the differential di-jet cross-section $\mathrm{d}\sigma/\mathrm{d}\log x_{\gamma,jets}$ in photoproduction at HERA are presented for rather low transverse jet energies. They reach parton fractional energies down to $x_{\gamma,jets} = 0.05$, a range where the gluons from the photon are found to dominate the di-jet cross-section. This kinematic region is strongly affected by underlying event energy and, for the $E_{T,jet} > 4$ GeV selection, by the uncertainties in the description of the transition from hard to soft processes. For di-jet events with $E_{T,jet} > 6$ GeV, where the cut is applied after subtraction of the underlying event energy, the correlation to the parton dynamics is greatly improved. Leading order QCD gives a good description of these data which makes possible a determination of the effective parton density in the photon. This quantity is dominated by the gluon density for $x_\gamma \leq 0.2$ which is found to rise strongly towards small x_γ. The result is in good agreement with earlier measurements of the H1 collaboration but more precise.

Acknowledgements

We are grateful to the HERA machine group whose outstanding efforts have made and continue to make this experiment possible. We thank the engineers and technicians for their work in constructing and now maintaining the H1 detector, our funding agencies for financial support, the DESY technical staff for continual assistance, and the DESY directorate for the hospitality which they extend to the non DESY members of the collaboration.

References

[1] H1 Collab., I. Abt *et al.*, *Phys. Lett.* **B 328** (1994) 176.

[2] H1 Collab., T. Ahmed *et al.*, *Nucl. Phys.* **B 445** (1995) 195.

[3] H1 Collab., C. Adloff *et al.*, *Eur. Phys. J.* **C 1** (1998) 97.

[4] ZEUS Collab., M. Derrick *et al.*, *Phys. Lett.* **B 384** (1996) 401;
ZEUS Collab., J. Breitweg *et al.*, *Eur. Phys. J.* **C 4** (1998) 591.

[5] H1 Collab., S. Aid *et al.*, *Z. Phys.* **C 70** (1996) 17.

[6] ZEUS Collab., J. Breitweg *et al.*, *Eur. Phys. J.* **C 11** (1999) 35.

[7] H1 Collab., I. Abt *et al.*, *Nucl. Instrum. Methods* **A 386** (1997) 310 and 348.

[8] H1 Collab., C. Adloff *et al.*, *Eur. Phys. J.* **C 13** (2000) 609.

[9] CDF Collab., F. Abe *et al.*, *Phys. Rev.* **D 45** (1992) 1448.

[10] PHOJET Monte Carlo, R. Engel, *Z. Phys.* **C 66** (1995) 203.

[11] T. Sjöstrand, CERN-TH-6488 (1992), *Comput. Phys. Commun.***82** (1994) 74.

[12] T. Sjöstrand, M. Bengtsson, *Comput. Phys. Commun.* **43** (1987) 367.

[13] M. Glück, E. Reya, A. Vogt, *Phys. Rev.* **D 46** (1992) 1973;
M. Glück, E. Reya, A. Vogt, *Z. Phys.* **C 53** (1992) 127.

[14] O. Kaufmann, *PhD Thesis Universität Heidelberg* 1999, unpublished.
http://www-h1.desy.de/psfiles/theses/h1th-185.ps

[15] G. D'Agostini, *Nucl. Instrum. Methods* **A 362** (1995) 487.

[16] B.L. Combridge and C.J. Maxwell, *Nucl. Phys.* **B 239** (1984) 429.

[17] R. Nisius, "The Photon Structure from Deep Inelastic Electron-Photon Scattering", hep-ex/9912049, accepted by Phys. Rep. C., Dec. 1999.

[18] ALEPH Collab., D.Barate *et. al.*, *Phys. Lett.* **B 458** (1999) 152;
DELPHI Collab., P.Abreu *et. al.*, *Z. Phys.* **C 69** (1996) 223;
L3 Collab., M.Acciarri *et. al.*, *Phys. Lett.* **B 447** (1999) 147;
OPAL Collab., K.Ackerstaff *et. al.*, *Z. Phys.* **C 74** (1997) 33;
for a review see [17].

[19] H1 Collab., C. Adloff *et. al.*, *Eur. Phys. J.* **C 10** (1999) 363.

[20] H. Abramowicz, K. Charchula, A. Levy, *Phys. Lett.* **B 269** (1991) 458.

[21] M. Glück, E. Reya, I. Schienbein, *Phys. Rev.* **D 60** (1999) 54019.

[22] G. A. Schüler, T. Sjöstrand, *Phys. Lett.* **B 376** (1996) 193.

	$E_{T,jet} >\ 4$ GeV			$E_{T,jet} >\ 6$ GeV		
$x_{\gamma,jets}$	$\frac{\mathrm{d}\sigma}{\mathrm{d}\log(x_{\gamma,jets})}[nb]$	stat.err.	total error	$\frac{\mathrm{d}\sigma}{\mathrm{d}\log(x_{\gamma,jets})}[nb]$	stat.err.	total error
0.053	0.49	0.03	0.14	0.06	0.02	0.03
0.094	0.88	0.04	0.22	0.17	0.03	0.06
0.16	0.92	0.04	0.24	0.17	0.03	0.06
0.25	0.83	0.04	0.14	0.21	0.03	0.06
0.40	0.85	0.04	0.17	0.29	0.04	0.09
0.71	0.78	0.04	0.14	0.54	0.05	0.14
0.93	0.54	0.04	0.12	0.47	0.06	0.12

Table 1: The γp di-jet cross-section $\mathrm{d}\sigma/\mathrm{d}\log(x_{\gamma,jets})$ corrected to hadron level with statistical and total error. Columns 2 to 4 give the cross-section for the kinematic range $E_{T,jet} >\ 4$ GeV, $M_{1,2}\ > 12$ GeV, $-0.5 < \eta_{jets} < 2.5,\ |\eta_{jet1} - \eta_{jet2}| < 1,\ 0.5 < y < 0.7$. The last three columns give the cross-section for $E_{T,jets} >\ 6$ GeV after pedestal energy subtraction in the kinematic range $-0.5 < \eta_{jets} < 2.5,\ |\eta_{jet1} - \eta_{jet2}| < 1\ ,\ 0.5 < y < 0.7$, $\eta_{jets} > -0.9 - \ln(x_{\gamma,jets})$.

x_γ	$\frac{1}{\alpha}x_\gamma f_{\gamma,eff}(x_\gamma)$	stat. error	total error	$\frac{1}{\alpha}x_\gamma g_\gamma(x_\gamma)$	stat. error	total error
0.053	10.1	3.3	4.9	4.0	1.4	2.1
0.094	6.6	1.1	2.0	2.4	0.5	0.9
0.17	3.5	0.3	1.2	0.99	0.12	0.55
0.30	2.2	0.1	0.5	0.34	0.03	0.30
0.50	2.3	0.2	0.8	0.33	0.08	0.40
0.79	2.1	0.1	0.4	0.02	0.03	0.33

Table 2: Columns 2 to 4: The effective parton density $f_{\gamma,eff} = (\ q(x_\gamma)\ + \bar{q}(x_\gamma) +\ 9/4\ g(x_\gamma)\ )$. Last three columns: The gluon density $g(x_\gamma)$. Both measurements are given for an average scale $\hat{p_t}^2 = 74$ GeV^2. Statistical and total errors are given separately.

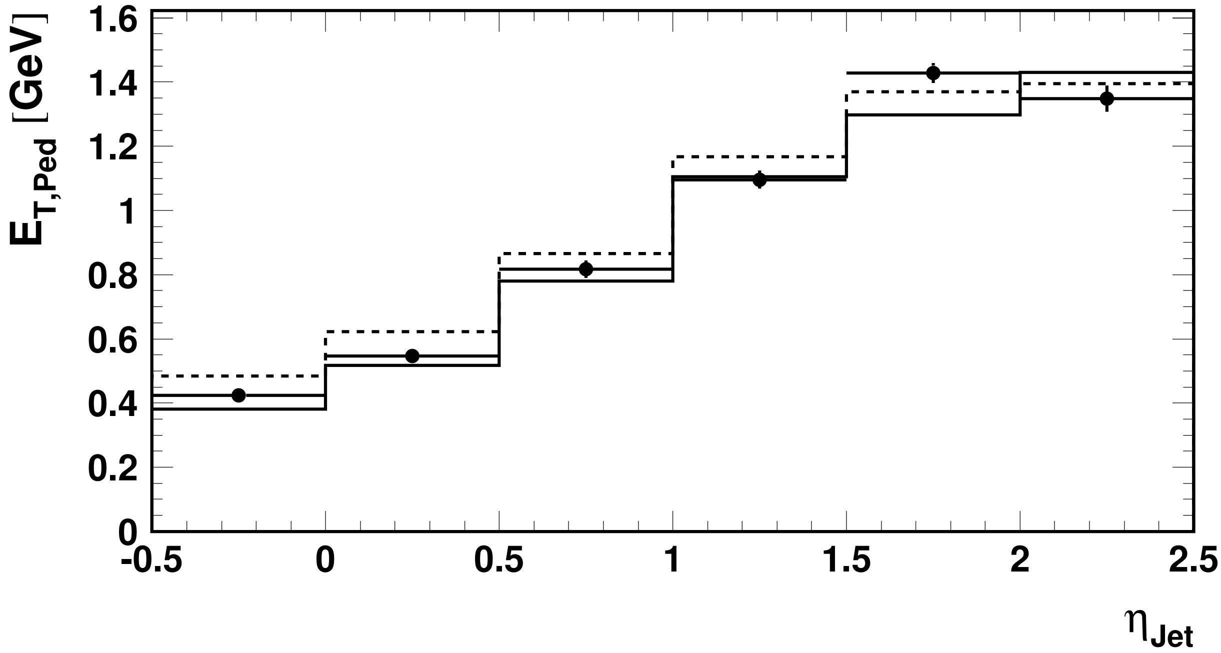

Figure 1: Mean transverse energy density (per unit area in $\eta - \phi$) outside of the jets (pedestal energy) evaluated in the interval $-1 < \eta - \eta_{jet} < 1$ as a function of jet pseudorapidity. The measured distribution at detector level (full circles with statistical error bars) is compared to the predictions of PYTHIA (dashed line) and PHOJET (full line).

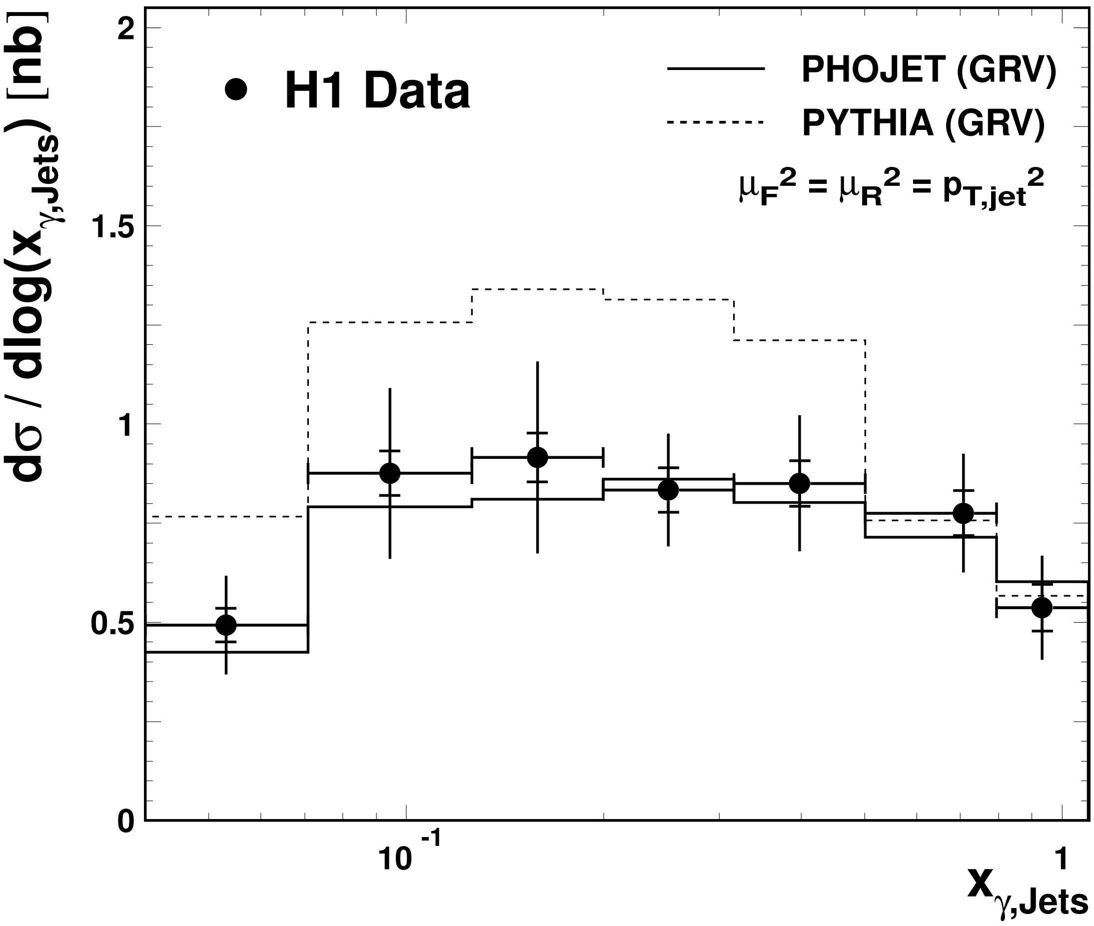

Figure 2: The di-jet cross-section at particle level (corrected for detector effects) as a function of $x_{\gamma,jets}$ in the kinematic range $E_{T,jet} > 4$ GeV, $M_{1,2} > 12$ GeV, $-0.5 < \eta_{jet} < 2.5,\ |\eta_{jet1} - \eta_{jet2}| < 1,\ 0.5 < y_e < 0.7$. The jets were reconstructed with a cone algorithm using $R = 0.7$. The inner error bars give the statistical error and the outer error bars give the total error. The data are compared to the predictions of PHOJET and PYTHIA using LO QCD matrix elements, the GRV92-LO parton density functions for photon and proton [13] and $\hat{p}_t$ for the factorisation scale μ_F and the renormalisation scale μ_R.

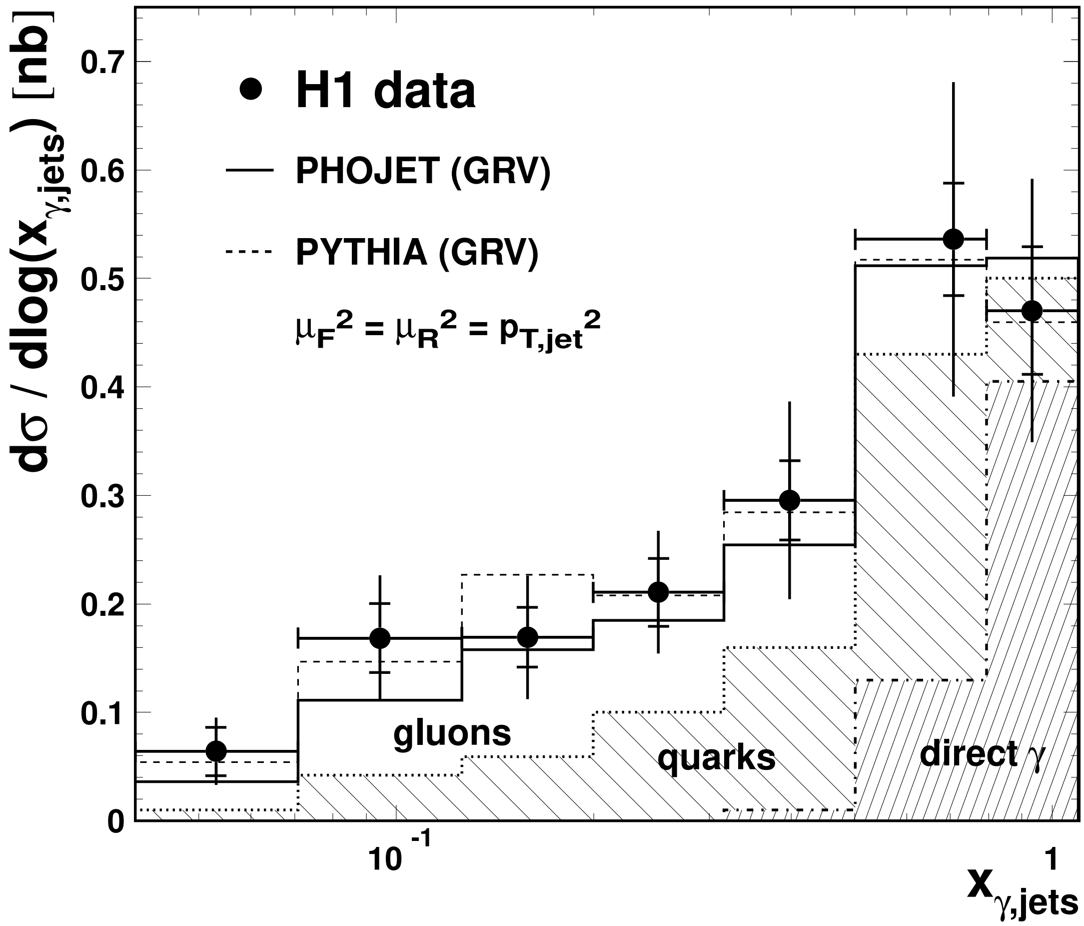

Figure 3: The di-jet cross-section at particle level (corrected for detector effects) as a function of $x_{\gamma,jets}$ for the data in the kinematic range $E_{T,jet} > 6$ GeV, $-0.5 < \eta_{jet} < 2.5$, $|\eta_{jet1} - \eta_{jet2}| < 1$, $\eta_{jets} > -0.9 - \ln(x_{\gamma,jets})$, $0.5 < y_e < 0.7$. The jets were reconstructed with a cone algorithm using $R = 0.7$. The transverse energy of the jets was required to be greater than 6 GeV after subtraction of the average pedestal energy. The inner error bars give the statistical error and the outer error bars give the total error. The data are compared to the LO QCD predictions of PHOJET and PYTHIA using the GRV92 LO parton density functions for photon and proton [13] and $\hat{p}_t$ for the factorisation scale μ_F and the renormalisation scale μ_R. The contribution of direct and resolved photon processes, as predicted by PHOJET, are also shown.

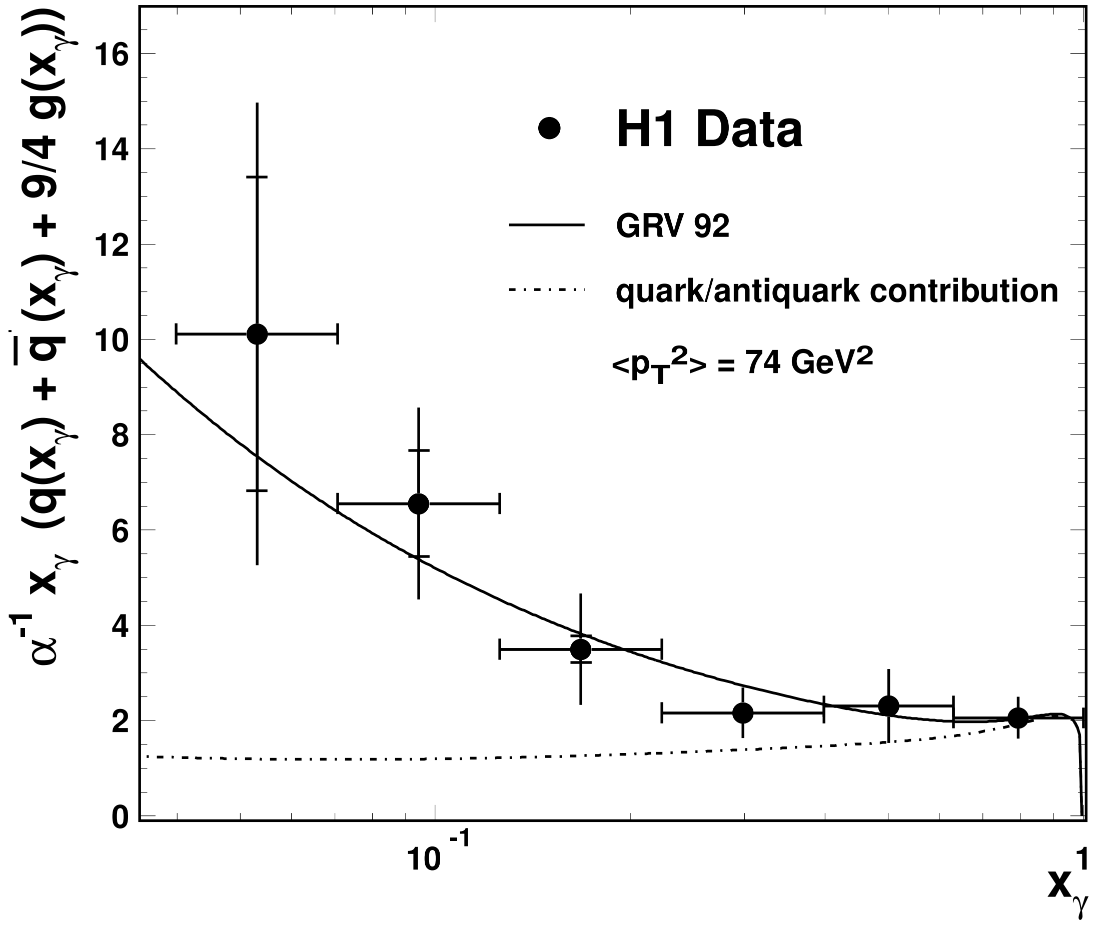

Figure 4: Effective parton distribution $f_{\gamma,eff} = (\ q(x_\gamma)\ + \bar{q}(x_\gamma) +\ 9/4\ g(x_\gamma)\ )$ of the photon multiplied by $\alpha^{-1}x_\gamma$ as a function of x_γ for a mean scale $\hat{p}_t^{\,2}\ =\ 74$ GeV^2 of the hard partons. The inner error bars give the statistical error and the outer error bars give the total error. The prediction based on the LO parametrisation of the parton distributions of the photon of GRV92-LO [13] is also shown as well as the sum of quark and antiquark contributions (dash-dotted curve).

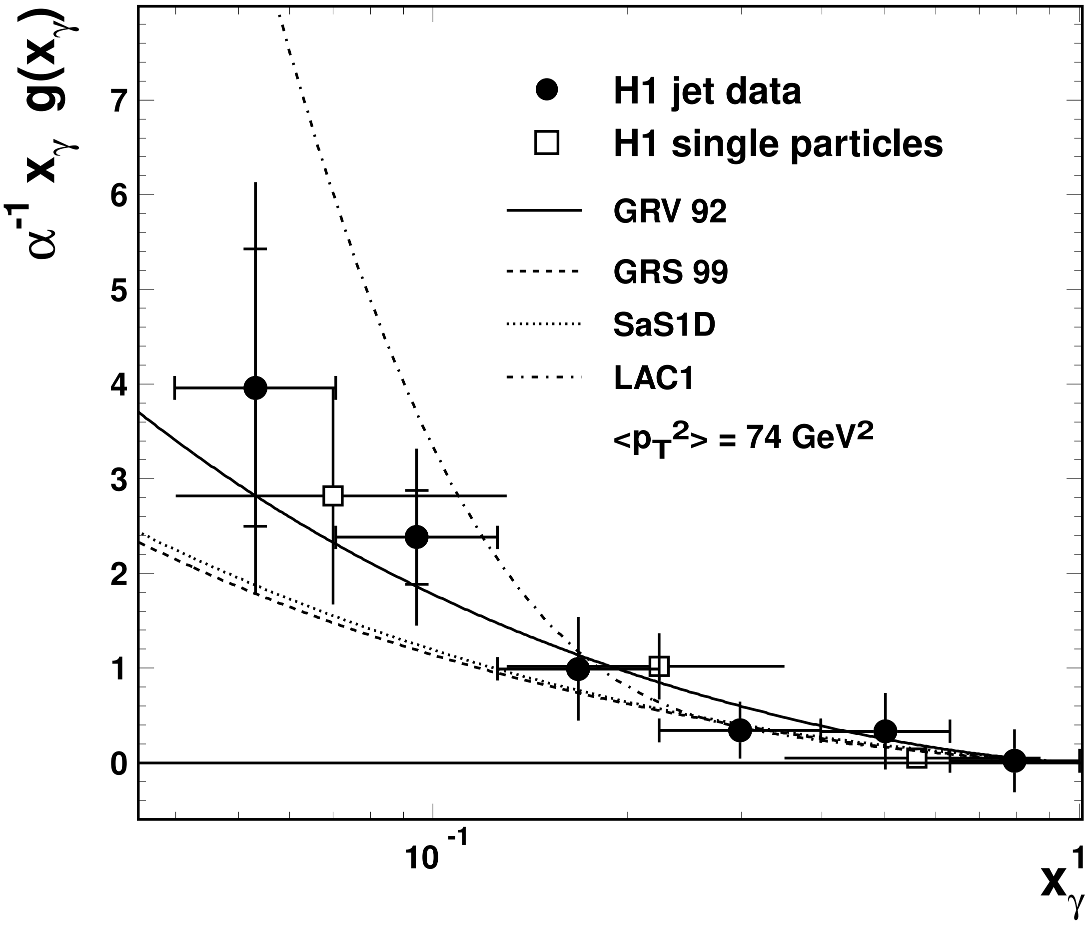

Figure 5: Gluon distribution $g(x_\gamma)$ of the photon multiplied by $\alpha^{-1}x_\gamma$ as a function of x_γ for a mean $\hat{p}_t^{\,2} = 74$ GeV^2 of the hard partons. The inner error bars give the statistical error and the outer error bars give the total error. The data points with open squares show a previous measurement of H1 which used single high E_T particles to determine the LO gluon density of the photon [19] at a mean scale $\hat{p}_t^{\,2} = 38$ GeV^2. The LO parametrisations of the gluon distribution [13, 20–22] based on fits to e^+e^- two-photon data are also shown.